Journal of Power Sources 181 (2008) 93–100

Contents lists available at ScienceDirect

Journal of Power Sources

journal homepage: www.elsevier.com/locate/jpowsour

Investigation of the performance decay of anodic PtRu catalyst with working time of direct methanol fuel cells

Zhen-Bo Wang[a,*], Xin-Peng Wang[b], Peng-Jian Zuo[a], Bo-Qian Yang[b], Ge-Ping Yin[a], Xian-Ping Feng[b]

[a] Department of Applied Chemistry, Harbin Institute of Technology, Harbin 150001, China
[b] Department of Physics, University of Puerto Rico, P.O. Box 23343, San Juan, PR 00931, USA

ARTICLE INFO

Article history:
Received 24 January 2008
Received in revised form 11 March 2008
Accepted 17 March 2008
Available online 25 March 2008

Keywords:
Direct methanol fuel cell
Life test
Anodic catalyst degradation
Electrochemically active surface area
In situ cyclic voltammetry

ABSTRACT

Life tests of direct methanol fuel cells (DMFC) were carried out with three individual single cells at a current density of 100 mA cm^{-2} for three different times under ambient pressure and at a cell temperature of 60 °C. X-ray diffraction (XRD) and X-ray photoelectron spectra (XPS) were used to characterize the anodic PtRu catalysts before and after the life tests. XRD results showed that the particle sizes of anodic catalysts increased from an original value of 2.8 to 3.0, 3.2, and 3.3 nm, whereas their lattice parameters first increased and then decreased from an original value of 3.8761 to 3.8879, 3.8777, and 3.8739 Å before and after 117, 210, and 312 working hours, respectively. XPS results indicated that during cells' working the contents of Pt and Ru oxides in anodic catalysts increased, but the metal content gradually decreased with test times. Polarization curves, power density curves, and *in situ* CO-stripping cyclic voltammetric (CV) curves were also plotted to evaluate the performances of fuel cells and electrochemically active surface areas (S_{EAS}) of anodic catalysts before and after life tests. After different time tests, the performances of DMFC lowered to different extents and could not recover their initial performances. The S_{EAS} of anodic catalyst decreased slightly by 4.78 and 9.03 $m^2 g^{-1}$ after 117 and 312 working hours, respectively. The utilization of anodic catalysts lowered slightly. This indicates that the change of (S_{EAS}) and utilization of anodic catalysts are not the main factors affecting the performance degradation of DMFC. The dissolution of Ru metal from anodic catalysts surface could be one of the main factors for the performance degradation of the PtRu black catalyst.

© 2008 Elsevier B.V. All rights reserved.

1. Introduction

Direct methanol fuel cells (DMFC) are attractive for several applications in view of their lower weight and volume compared with indirect fuel cells [1]. Investigations of DMFC are mainly focused on the catalysts [2,3], methanol crossover [4–6], carbon support [7,8], Nafion modification [9], the optimization of gas electrode layer [10], and so on in the past decades. Significant advances have been made for DMFC developments [11–13]. But, at present, their performance cannot meet the demand of DMFC commercialization. In addition, the cost of DMFC is still high because of the expensive noble metals of Pt and Ru used as catalysts in cathodes and anodes. The resource of platinum is limited, and that of ruthenium is very rare, limiting the commercialization of DMFC as well. Hence, it is very worth enhancing the activity and prolonging the life of catalysts for DMFC and lowering the cost of DMFC by using new techniques. The performance degradation rates of DMFC, generally higher than that of hydrogen PEMFC, are typically in the range of 10–25 μV h^{-1} [14]. The commercialization of DMFC demands a stable operation for at least thousands of hours, e.g. 5000–40,000 h usually required for fuel cell vehicles and residential power generators, which is not easy to achieve [15]. Most of the fundamental mechanisms determining the life of DMFC are poorly understood, such as membrane electrode assembly (MEA) failure mechanisms including the growth and corrosion of catalytic particles resulting in compositional changes, poisoning of electrocatalysts by accumulated intermediates from methanol electro-oxidation or impurities, the aging of polymer electrolyte membrane, and changes in the hydrophobic/hydrophilic properties in the catalyst layers and diffusion layers [16,17]. Preliminary research results indicated that the electrocatalysts' stability plays an important role in the long-term operation of fuel cells [18]. The degradation of catalysts in DMFC proceeds gradually, and its degree is time-dependent. DMFC cathodes operate in a more corrosive environment of high water content, low pH value (<1), high temperature (50–90 °C), and high potentials (0.6–1.2 V) coupled with operating oxygen partial pressures [19]. The carbon support can also be oxidized in the case of fuel starvation [14]. So, the agglomeration and dissolution of the catalyst

* Corresponding author. Tel.: +86 451 8641 7853; fax: +86 451 8641 3707.
E-mail address: wangzhenbo1008@yahoo.com.cn (Z.-B. Wang).

0378-7753/$ – see front matter © 2008 Elsevier B.V. All rights reserved.
doi:10.1016/j.jpowsour.2008.03.042

in cathodes are more serious than that in anodes. Some research results showed, however, that the agglomeration of catalyst in anodes is more serious than that in cathodes, because methanol might be more aggressive towards the catalyst than water produced in DMFC [20]. With respect to the agglomeration of catalysts, there are two mechanisms for particle size growth, i.e. Ostwald ripening and coalescence [21–25]. Although coalescence has been reported to be insignificant for carbon supported catalysts at temperatures below 500 °C, or in a gas phase [22], this may not be the case with DMFC where metal black catalysts are typically used. The primary growth mechanism, i.e. Ostwald ripening, would be expected to be more serious at the cathode [24]. However, the aging intrinsical mechanism of anodic catalysts is not clear, the changing characteristics of PtRu with time during DMFC operation are not discussed in detail yet. It is necessary to explore the aging regularity and its mechanism for anodic catalysts at different periods of time. In the present paper, we carry out the short-term life tests of DMFC of 117, 210, and 312 h, respectively, with three single DMFC operated at 60 °C using Johnson Matthey unsupported Pt and PtRu catalysts. Electrochemical characterizations of anodic catalysts were performed, the results of X-ray diffraction (XRD) and X-ray photoelectron spectra (XPS) characterizations obtained prior to and after tests were discussed.

2. Experimental

2.1. MEA preparation

Johnson Matthey Pt black and PtRu black (Johnson Matthey Co.) were used as catalysts for the cathode and anode, respectively. PtRu black and 5 wt.% Nafion® ionomer solution (DuPont Co., EW = 1100) were mixed in isopropanol alcohol solution to form a homogeneous catalyst black suspension for the anode. The cathodic catalyst ink was prepared similarly with Pt black, Nafion® ionomer, and PTFE latex. The Nafion® contents in both anodic and cathodic catalyst layers were 20 wt.%. The catalyst inks were deposited onto the gas diffusion layers (GDLs) by paint brush with a metal loading of 4 mg cm^{-2} for both electrodes. The carbon cloth (E-TEK, ELAT/NC/DS/V2 double-sided ELAT electrode, carbon only-no metal, 20% wet proofed) was used as the GDL and backing layer for the cathode. The anodic GDL was prepared by using spray painting method with a carbon black of 1 mg cm^{-2} and 5% Nafion® ionomer solution on the carbon paper (Toray paper TGPH 060). DuPont Nafion® 117 membrane was used as the solid electrolyte. Before being applied to the electrodes, the membrane was pretreated by diluted nitric acid (the ratio of nitric acid/deionized water of 18 MΩ cm by volume is 1:1) at its boiling temperature for 20 min and then rinsed five times with ultrapure water. The membrane was then immersed in the boiling ultrapure water for 1 h. The membrane electrode assembly was formed by hot-pressing the anodic and cathodic diffusion layers onto the Nafion® film.

2.2. Electrochemical measurements

2.2.1. Single fuel cell tests

Single fuel cell tests were performed by using a homemade 5 cm^2 apparent area test fixture. The fixture was composed of a pair of graphite plates with serpentine flow fields for reactants to flow. Air and methanol solution were used as the reactants. The flow rate of air is 100 mL min^{-1} under ambient pressure, and that of methanol solution is 2.5 mL min^{-1} with a concentration of 1.0 mol L^{-1} methanol. Both reactants were not humidified, and directly enter the cell. The cell temperature was 60 °C. Rod-like heaters were inserted into the plates to control the cell temperature. Polarization curves, power density curves, and potential–time curves were obtained by using a Fuel Cell Test Station (Scribner Associates Inc., Series 890B, Southern Pines, NC, USA) in a galvanostatic mode. Potential–time curves of the three single cells were plotted in a galvanostatic mode with a current density of 100 mA cm^{-2} for 117, 210, and 312 h, respectively. To ensure that the electrolyte in the Nafion membrane and electrode is moist enough to have high ionic conductivity, it is necessary to activate the MEA before the performance measurements. In our experiment, the single cells were conditioned with ultrapure water and air at 60 °C for 5 h. After conditioning, ultrapure water was replaced with methanol solution of 1.0 mol L^{-1} for 24 h in a galvanostatic mode with a current density of 10 mA cm^{-2} prior to the acquisition of life data. The cell voltage gradually increases with time during conditioning.

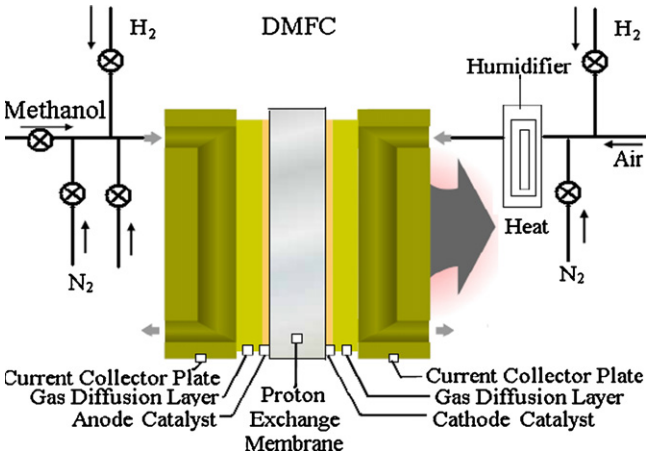

Fig. 1. Schematics of fuel cell set-up including alteration for CV measurements. For CO stripping, methanol solution at the anode was purged with humidified N_2 for 10 min, and then nitrogen was replaced with CO for 15 min, and again nitrogen was used to scavenge the residual CO in the chamber. The original anode became the working electrode and air at the cathode was purged with N_2 for 10 min, and then N_2 was replaced with humidified H_2. The cathode became the counter/reference electrode.

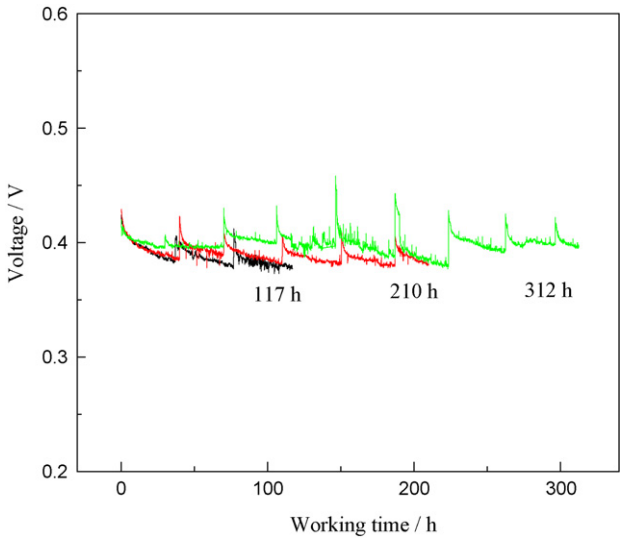

Fig. 2. Life tests of DMFC by using three single cells with an apparent cross-sectional area of 5 cm^2 for different times. Anodic catalyst: PtRu black, metal loading 4 mg cm^{-2}. Cathodic catalyst: Pt black, metal loading 4 mg cm^{-2}. Operating conditions: 60 °C, 100 mA cm^{-2}. Anodic feed: 1.0 mol L^{-1} CH_3OH solution with a flow rate of 2.5 mL min^{-1}. Cathodic feed: air at ambient pressure with a flow rate of 100 mL min^{-1}.

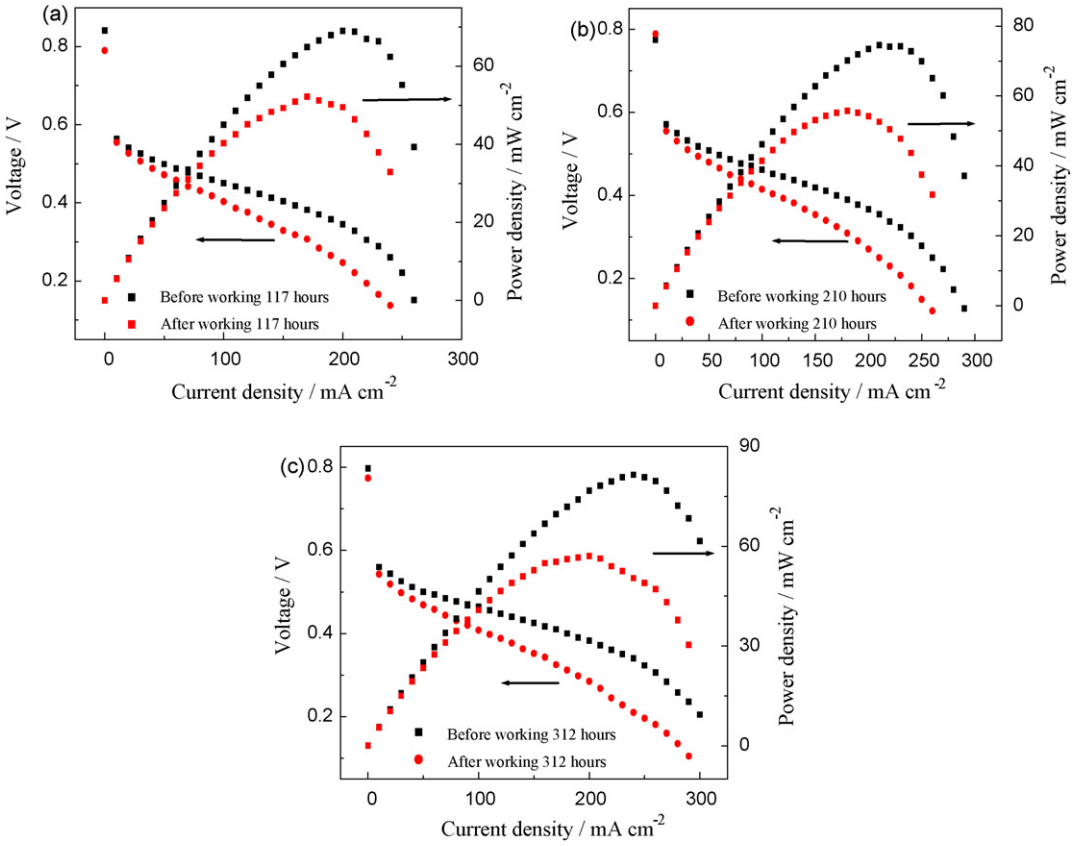

Fig. 3. Performances of three single DMFC before and after different test times. Temperature: 60 °C. Anodic feed: 1 mol L^{-1} CH_3OH solution with a flow rate of 2.5 mL min^{-1}; cathode feed: air at ambient pressure with a flow rate of 100 mL min^{-1}.

2.2.2. Cyclic voltammetry (CV)

Cyclic voltammograms were obtained by using a PAR potentiostat/galvanostat (EG&G Model 273A) at a cell temperature of 25 °C. Fig. 1 shows a scheme of the experimental set-up for fuel cell testing and *in situ* cyclic voltammetric measurements. Electrochemically active surface areas (S_{EAS}) of anodic catalysts were determined by CO-stripping measurement. For this, the fuel cell cathode was served as both reference (defined as a dynamic hydrogen electrode (DHE)) and counter electrodes by first purging the cathode with nitrogen for 10 min, and then switching to humidified hydrogen at a flow rate of 100 mL min^{-1} and ambient pressure. The anode was taken as a working electrode, and first was purged with nitrogen for 10 min, and then replaced with CO for 15 min, and purged again with nitrogen to the chamber for 10 min. The potential was scanned at a rate of 0.02 V s^{-1} between 0.05 and 1.2 V. The integrated peak area of CO electro-oxidation was used to calculate the S_{EAS} of anodic catalyst. All potential values reported in this work are versus DHE.

2.3. Characterization of physical properties

After electrochemical testing, the MEA was carefully removed from the cell. The anodes GDLs were separated from the MEAs at different test times. The membranes with catalyst layers were cut into smaller pieces for the subsequent analysis by XRD and XPS.

2.3.1. X-ray diffraction (XRD)

XRD measurements for the catalyzed GDL were made with a Rigaku Ultima III X-ray diffractometer system (Rigaku MSC, Woodlands, TX) using a graphite crystal counter monochromator that filtered Cu Kβ radiation. The X-ray source was operated at 40 kV and 40 mA. The patterns, recorded in a 2θ range of 20–140°, were

Table 1
Maximum power densities (MPD), voltages, and current densities at MPD of the membrane electrode assemblies before and after different test times

Membrane electrode assembly	117 h		210 h		312 h	
	Before	After	Before	After	Before	After
Current density at MPD (mA cm^{-2})	200	170	210	180	240	200
Decrease (mA cm^{-2})	30		30		40	
Voltage at MPD (V)	0.345	0.307	0.355	0.309	0.34	0.285
Decrease (mV)	38		46		55	
MPD (mW cm^{-2})	69.0	52.2	74.5	55.7	81.5	57.0
Decrease (mW cm^{-2})	16.8		18.8		24.5	
Changing rate (%)	24.3		25.2		30.1	

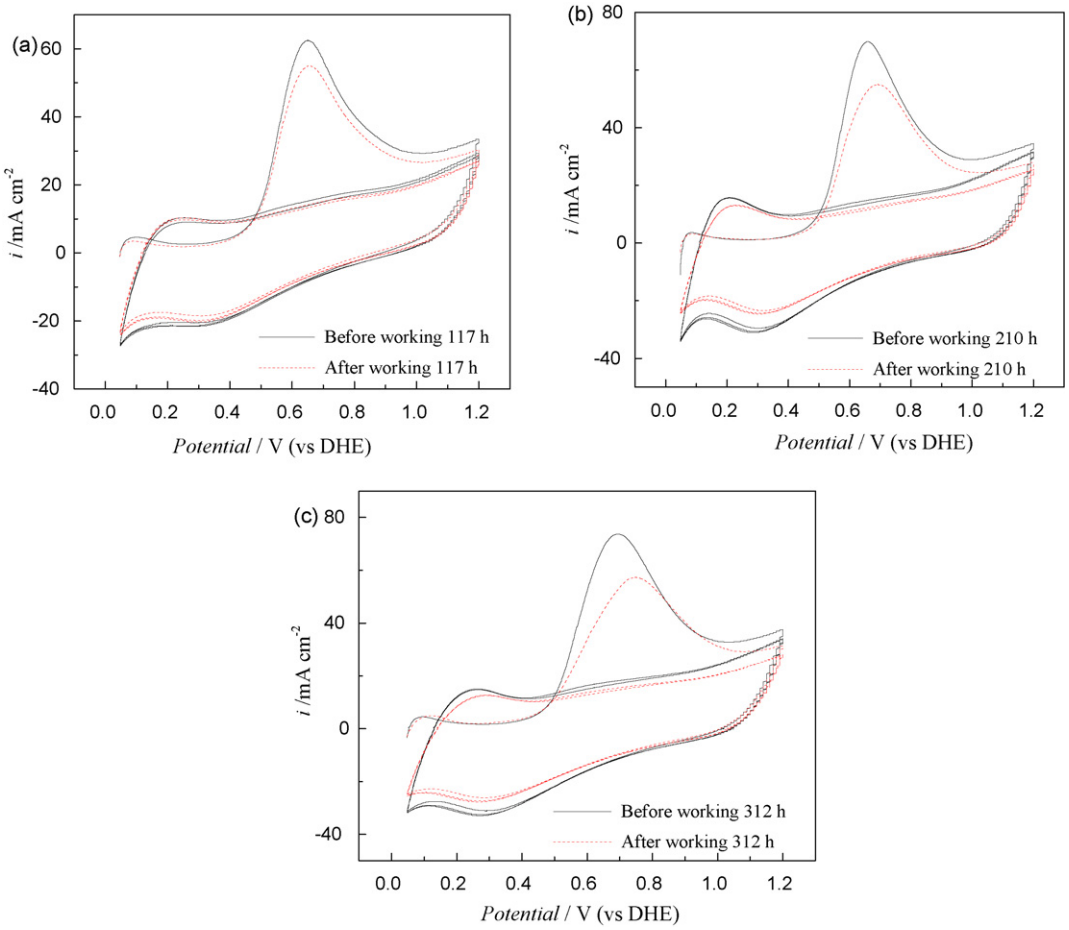

Fig. 4. CO-stripping test of anodic catalysts before and after different times. Temperature: 25 °C. (a) 117 h; (b) 210 h; (c) 312 h.

obtained using high precision and high resolution parallel beam geometry in a step scanning mode of 1 deg min^{-1}. The identification of phases was made by referring to the joint committee on powder diffraction standards international center for diffraction data (JCPDS-ICDD) database. Lattice parameters and crystallite sizes were calculated using Jade 7 Plus software (Rigaku). Grain sizes were determined from the Scherrer equation using the Pseudo-Voigt profile function.

2.3.2. X-ray photoelectron spectrometry (XPS)

XPS study of surface composition involved a special X-ray photoelectron spectrometer (VG ESCALAB MKII) with the Al Kα X-ray source of 1486.6 eV, which recorded the spectra from the takeoff-angle of 45° at a chamber pressure below 5×10^{-9} Pa. The C 1s electron binding energy was referenced at 284.6 eV, and a non-linear least-squares curve-fitting program was employed with a Gaussian–Lorentzian production function [26,27]. The deconvolution of the XPS spectra was achieved with the reported procedures [28–32].

3. Results and discussion

The life tests of three single cells were carried out at a cell temperature of 60 °C at 100 mA cm^{-2}. As shown in Fig. 2, during each continuous discharge process, the majority of voltage losses occur in the first few hours and then its decline becomes less sig-

Table 2
Different parameters of anodic catalysts before and after different test times

Working times (h)	117		210		312	
	Before	After	Before	After	Before	After
Peak potential for CO oxidation (V)	0.649	0.650	0.655	0.690	0.689	0.744
S_{EAS} (m^2 g^{-1})	39.97	35.19	42.52	35.74	49.52	40.49
Onset potential for CO oxidation	0.506	0.508	0.503	0.499	0.484	0.483
S_{EAS} changing (m^2 g^{-1})	4.78		6.78		9.03	
Changing rate (%)	12.0		15.9		18.2	
d_{XRD} (nm)	2.8	3.0	2.8	3.2	2.8	3.3
d_{XRD} changing (nm)	0.2		0.4		0.5	
S_{XRD} (m^2 g^{-1})	109.9	102.6	109.9	96.2	109.9	93.2
S_{XRD} changing (m^2 g^{-1})	7.3		13.7		16.7	
Changing rate (%)	6.6		12.5		15.2	
Utilization of catalysts (%)	36.4	34.3	38.7	37.2	45.1	43.4
Lattice parameters (Å)	3.8761	3.8879	3. 8761	3.8777	3.8761	3.8739

nificant. The initial rapid performance loss was attributed to the non-equilibrium state among ruthenium oxides [33,34]. During the life tests, continuous discharges were interrupted by refilling the methanol solution, resulting in the performance recovery of DMFC to nearly the initial values for the next discharge. The recovery should be attributed to the oxidation purge of methanol crossover from anode to cathode. The over-potential of the cathode is very high, when the DMFC is working. Therefore, the methanol from anode is not entirely oxidized at the cathode. The methanol and/or intermediates of its oxidation can be accumulated in the cathode, which slowly poison the Pt catalyst and gradually deteriorate the performance of DMFC. The potential of cathode is very high when the DMFC stopped working, and the accumulated methanol/intermediates are entirely oxidized. It causes that the performance of DMFC recovers nearly to the initial value when it is started again. During the whole test process, the cell voltages decrease with test time, there is a slow performance loss that is irrecoverable, which might relate to the degradation of catalysts, the dissolution of Nafion® solution in the catalyst layers [35], and the aging of polymer electrolyte membrane [17]. The voltage decay rates of DMFC are about 0.4, 0.22, and 0.07 mV h^{-1} during the tests for 117, 210, and 312 h, respectively. It can be seen that the voltage decay rates decrease evidently with time. Though, the decay rate for 312 h is already close to that for commercialization demands (within a range of 10–25 μV h^{-1}) of DMFC. It is still by three to seven times greater than that of the demands [14]. It is quite necessary to do hard works to prolong the operating life of DMFC.

The cell performances before and after the life tests were compared by polarization and power density curves of the three single cells recorded at a temperature of 60 °C with cathodes fed with air under ambient pressure as shown in Fig. 3. The cell performances have different extents of decay with test time. Their correlative data are listed in Table 1. Compared with the cell performances before tests, it can be seen that the maximum power densities (MPD) of DMFC drop 24.3, 25.2, and 30.1% after a test time of 117, 210, and 312 h, respectively. The current densities and potentials, at which the MPD occur, also drop with test times. The loss of cell voltage at which MPD occurs has the highest value of approximately 55 mV after the life test of 312 h. Its loss of power density at a cell voltage of 0.4 V is also the highest, about 39.2%. Furthermore, the decrements of the cell voltages after life tests at the same current densities increase with increasing of current densities during the life tests as shown in Fig. 3, compared with those before the tests.

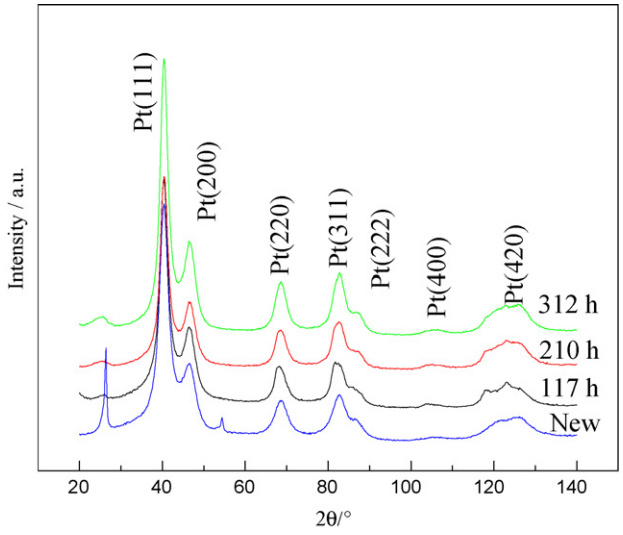

Fig. 5. XRD patterns of anodic catalysts before and after different test times.

Fig. 4 shows CO adsorption–oxidation curves in anodes before and after the life tests for different times. The onset potentials and peak potentials of CO adsorption–oxidation are listed in Table 2. It can be seen from Fig. 4 that the hydrogen region peaks are almost completely suppressed in the first scan-cycle, as CO molecules were adsorbed onto the catalyst, which restrained the hydrogen-desorption. After the life test, the onset potentials and peak potentials of CO adsorption–oxidation are shifted to a higher potential as presented in Table 2. Generally, the change in the catalyst composition manifests itself more remarkably for the CO-stripping curves [36]. This result indicates that Ru metal is dissolved from the catalyst during the operation, and the loss of Ru metal increases with the test time.

The electrochemically active surface area (S_{EAS}), which reflects the intrinsic electrocatalytic activity of a catalyst, is calculated with the recognized method based on the CO-stripping voltammetry curve [37,38], through Eq. (1) as follows:

$$S_{EAS} = \frac{Q_1}{G \times Q_{CO}} \quad (1)$$

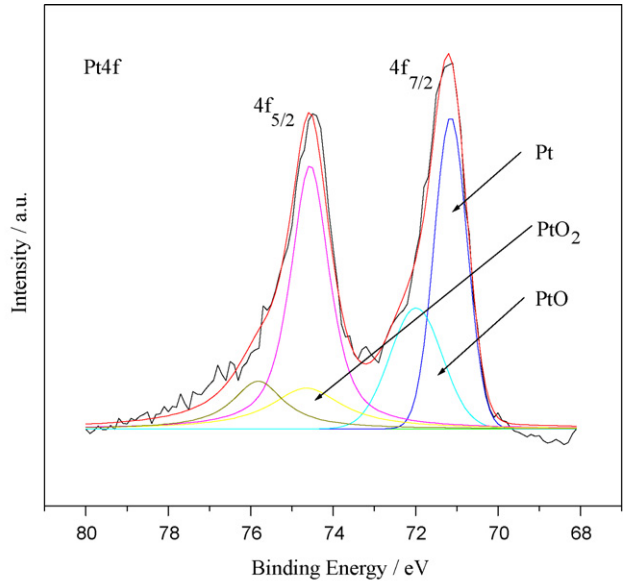

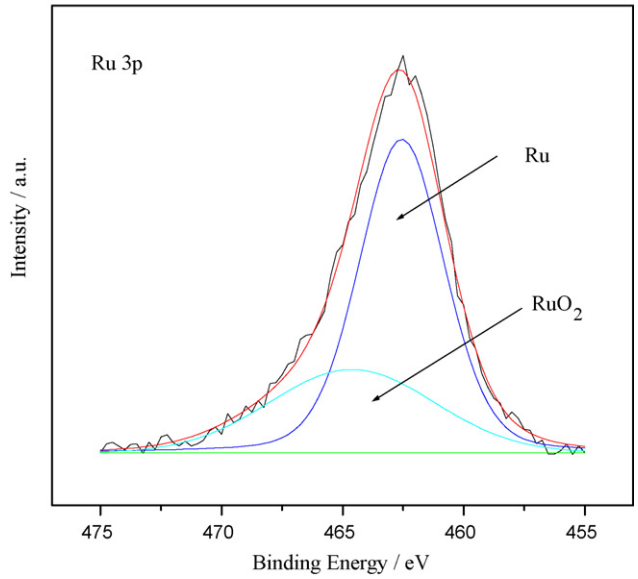

Fig. 6. XPS core level spectra of anodic catalyst before life test.

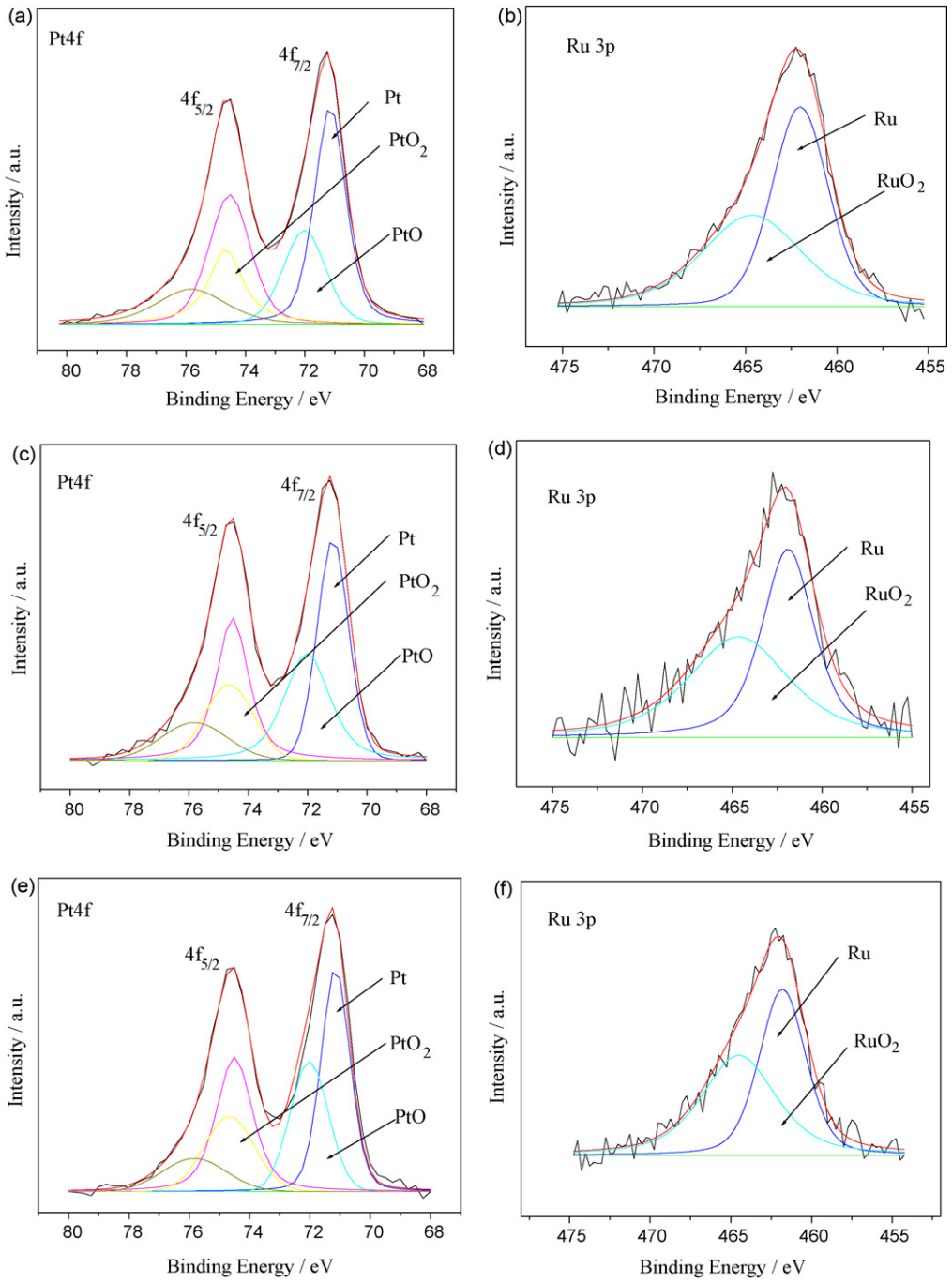

Fig. 7. XPS core level spectra of anodic catalyst after different test times Pt 4f after 117 h; (b) Ru 3p after 117 h; (c) Pt 4f after 210 h; (d) Ru 3p after 210 h; (e) Pt 4f after 312 h; (f) Ru 3p after 312 h.

where Q_1 is the charge quantity calculated from integrated in CV curves for CO desorption electro-oxidation in microcoulomb (μC), and Q_{CO} is the charge required to oxidize a monolayer of CO on the alloy catalyst of 420 (μC cm^{-2}) [39], and G represents the total metal loading (mg) in the electrodes.

The S_{EAS} calculations of anodic catalysts are listed in Table 2. The S_{EAS} of anodic catalysts decrease with time. The S_{EAS} loss after test times of 117, 210, and 312 h are by 12.0, 15.9, and 18.2%, respectively. The increments in loss decrease with time. However, the changes of S_{EAS} are evident, the variations of catalysts' utilization (S_{EAS}/S_{XRD}) for anodes are almost the same, by about 1–2% before and after the life tests as presented in Table 2. Those results are in good agreement with our previous work [40]. The results also indicate that the 'triple-phase boundaries' where the electrolyte, reaction materials, and electrically connected catalyst particles contact together in anodes, are not markedly decreasing after the life tests. Namely, the performance decays of DMFC due to the aging of anodic catalysts are insignificant.

After the single cell tests, the used MEAs were separated carefully and cut into small pieces for further analysis. XRD patterns of anodes were shown in Fig. 5.

The diffraction peaks at 26° observed for anodes can be attributed to the hexagonal graphite structures (0 0 2) of the carbon black remaining on the catalyst layer after peeling off from

Table 3
Surface contents of Pt and Ru metal, and their oxide in anodic catalysts before and after different test times

Materials	Compositions	New catalyst	After 117 h	After 210 h	After 312 h
Pt	Pt	62.0	56.7	55.0	54.4
	PtO	28.3	28.5	29.6	29.6
	PtO_2	9.7	14.8	15.4	16.0
Ru	Ru	68.4	53.1	49.4	48.6
	RuO_2	31.6	46.9	50.6	51.4

the GDLs. The PtRu black has a face-centered cubic (fcc) structure showing the major peaks of (1 1 1), (2 0 0), (2 2 0), (3 1 1), (2 2 2), and (4 0 0). The mean particle sizes and lattice parameters of the catalysts before and after life tests were calculated from XRD patterns by using JADE software. Their results are listed in Table 2. It can be seen from Table 2 that the particle sizes and lattice parameters of anodic catalysts grow from an initial value of 2.8 to 3.0, 3.2, and 3.3 nm, and from an initial value of 3.8761 to 3.8879, 3.8777, and 3.8739 Å before and after 117, 210, and 312 h of tests, respectively. The slow sintering rate of the anodic catalysts may be due to the relative low over-potential and oxygen concentration for anodes during their operation. This is consistent with Xin's result [17]. Yi and coworkers [20] thought that methanol might be more aggressive towards electrocatalysts than water. However, the effect of methanol on the aging of anodic catalysts is weak in our work. Although small unsupported Pt particles are unstable in an electrochemical environment due to sintering during the operation [41], the growth rate of anodic catalysts with smaller particle size are relatively small with test time in the present work. In addition, the lattice parameter of the PtRu alloy catalyst increases due to the oxidation, dissolution, and separation of Ru metal atoms in the Pt crystalline lattices, which make the molar ratio of Pt and Ru in PtRu alloy deviate from the nominal value of 1:1. This result is consistent with that of CO-stripping curves for anodes. So, the onset potential and peak potential of CO electro-oxidation are shifted to positive potential after the life test as shown in Table 2.

The specific surface area of catalysts (denoted as S_{XRD}) calculated from XRD patterns are also listed in Table 2. The S_{XRD} of anodic catalyst decreases with time. Compared with the S_{EAS}, the loss rate of S_{XRD} is smaller than that of the S_{EAS}. This interprets that it might be other factors, such as the dissolution of Nafion® ionomer reducing the S_{EAS} besides the agglomeration of anodic catalyst. The Nafion with catalyst particles in it desquamates and/or dissolves in the catalyst layer due to their growth, thus results in the decreasing of the proton conduction paths and 'triple-phase boundaries', and the S_{EAS} loss is relatively high.

Figs. 6 and 7 present that the curve-fitted Pt 4f XPS and Ru 3d spectra of PtRu black anodic catalysts before and after different test times, respectively. The oxidation states of Pt, Ru, and their relative amounts obtained from XPS measurements are listed in Table 3.

The metal contents of Pt and Ru in PtRu black decrease after the life tests. The oxides content of Pt and Ru increase evidently with test times after the life tests. The decrease of Pt metal content after a test of 312 h is relatively low, by about 7.6%. Meanwhile, the decrease of Ru metal content after the test is substantially more, by about 19.8%. The similar results are obtained after the tests of 117 and 210 h.

The increase of Pt(II) oxide amounts after life tests are small. Furthermore, the Pt(IV) oxide amounts slowly increase with test times. It is reasonable to expect that the Pt nanoparticles during the life tests are not easily oxidized, dissolved and then redeposited to grow under the lower polarization potential and less oxygen-containing species in anodes than those in cathodes. However, the Ru metal content after the life tests rapidly decreases with test times, and meanwhile the Ru(IV) oxide contents with test times sharply increase. The relative peak area of Pt(II), Pt(IV), and Ru(IV) for the PtRu anode alloy does not change after the durability tests. It can be believed that the Ru metal in anodic PtRu black catalyst during its operation is more easily oxidized and dissolved, which lowers the potential for Pt metal dissolution and reduce the loss of Pt metal. Simultaneously, the hydrous oxide of Ru during the operation is in favor of supporting more oxygen-containing (–OH) species and improving methanol electro-oxidation [42]. These factors make PtRu alloy catalyst exhibit a highly stable electrocatalytic activity towards methanol electro-oxidation.

4. Conclusions

Life tests of three single cells of direct methanol fuel cells were carried out at a current density of 100 mA cm^{-2} under ambient pressure and a cell temperature of 60 °C. After the long period of operations and tests, the performances of the DMFC lowered to different extents and could not recover the initial performance. The losses of their initial maximum power densities increased with their operation times. After running for more than several hundreds of hours, the particle sizes of catalysts augmented with test times. The contents of Pt and Ru oxides in the anodic catalysts increased, and the metal amount decreased with operation times. The existence of Ru oxide or hydroxide in the anodic catalyst layer hinders the dissolution of Pt and the agglomeration of catalyst particles. The dissolution of Ru metal and the aging of anodic catalyst contributing to the performance degradation of DMFC are relatively small. However, the dissolution of Ru metal from anodic catalyst surface could be one of the main factors to the performance degradation of the PtRu black catalyst.

Acknowledgements

This work is supported financially by the National Natural Science Foundation of China (Grant No. 20606007), Postdoctoral Science-Research Developmental Foundation of Heilongjiang Province of China (LBH-Q07044), the Scientific Research Foundation for the Returned Overseas Chinese Scholars, State Education Ministry (2008) and Harbin Innovation Science Foundation for Youths (2007RFQXG042).

References

[1] A. Heinzel, V.M. Barragan, J. Power Sources 84 (1999) 70–74.
[2] J.H. Choi, K.W. Park, I.S. Park, K. Kim, J.S. Lee, Y.E. Sung, J. Electrochem. Soc. 153 (2006) A1812–A1817.
[3] K. Han, J. Lee, H. Kim, Electrochim. Acta 52 (2006) 1697–1702.
[4] N. Munichandraiah, K. McGrath, P.G.K. Surya, R. Aniszfeld, G.A. Olah, J. Power Sources 117 (2003) 98–101.
[5] B. Gurau, E.S. Smotkin, J. Power Sources 112 (2002) 339–352.
[6] R.Z. Jiang, C. Rong, D. Chu, J. Electrochem. Soc. 154 (2007) B13–B19.
[7] B.S. Xu, X.W. Yang, X.M. Wang, J.J. Guo, X.G. Liu, J. Power Sources 162 (2006) 160–164.
[8] J.L. Figueiredo, M.F.R. Pereira, P. Serp, P. Kalck, P.V. Samant, J.B. Fernandes, Carbon 44 (2006) 2516–2522.
[9] A.H. Tian, J.Y. Kim, J.Y. Shi, K. Kim, K. Lee, J. Power Sources 167 (2007) 302–308.
[10] J. Zhang, G.P. Yin, Z.B. Wang, Y.Y. Shao, J. Power Sources 160 (2006) 1035–1040.
[11] A.K. Shukla, C.L. Jackson, K. Scott, G. Murgia, J. Power Sources 111 (2002) 43–51.
[12] D. Kim, J. Lee, T.H. Lim, I.H. Oh, H.Y. Ha, J. Power Sources 155 (2006) 203–212.
[13] Z.B. Wang, G.P. Yin, P.F. Shi, Carbon 44 (2006) 133–140.
[14] S.D. Knights, K.M. Colbow, J. St-Pierre, D.P. Wilkinson, J. Power Sources 127 (2004) 127–134.
[15] S.Y. Ahn, S.J. Shin, H.Y. Ha, S.A. Hong, Y.C. Lee, T.W. Lim, I.H. Oh, J. Power Sources 106 (2002) 295–303.
[16] K. Washington, Fuel cell seminar abstracts, Portland, 2000, p. 468.
[17] W.M. Chen, G.Q. Sun, J.S. Guo, X.S. Zhao, S.Y. Yan, J. Tian, S.H. Tang, Z.H. Zhou, Q. Xin, Electrochim. Acta 51 (2006) 2391–2399.
[18] L.H. Jiang, G.Q. Sun, S.L. Wang, G.X. Wang, Q. Xin, Z.H. Zhou, B. Zhou, Electrochem. Commun. 7 (2005) 663–668.
[19] Y.Y. Shao, G.P. Yin, Y.Z. Gao, P.F. Shi, J. Electrochem. Soc. 153 (2006) A1093–A1097.

[20] J.G. Liu, Z.H. Zhou, X.X. Zhao, Q. Xin, G.Q. Sun, B.L. Yi, Phys. Chem. Chem. Phys. 6 (2004) 134–137.
[21] P. Ascarelli, V. Contini, R. Giorgi, J. Appl. Phys. 91 (2002) 4556–4561.
[22] J.A. Bett, K. Kinoshita, P. Stonehart, J. Catal. 35 (1974) 307–316.
[23] J.A.S. Bett, K. Kinoshita, P.J. Stonehart, J. Catal. 41 (1976) 124–133.
[24] P.J. Ferreira, La OF G.J., Y. Shao-Horn, D. Morgan, R. Makharia, S. Kocha, H.A. Gasteiger, J. Electrochem. Soc. 152 (2005) A2256–A2271.
[25] C.G. Granqvist, R.A. Buhrman, J. Catal. 42 (1976) 477–479.
[26] K.W. Park, J.H. Choi, B.K. Kwon, S.A. Lee, Y.E. Sung, H.Y. Ha, S.A. Hong, H.S. Kim, A. Wieckowski, J. Phys. Chem. B 106 (2002) 1869–1877.
[27] C. Bock, C. Paquet, M. Couillard, G.A. Botton, B.R. MacDougall, J. Am. Chem. Soc. 126 (2004) 8028–8034.
[28] F.J. Rodriguez-Nieto, T. Morante-Catacora, C.R. Cabrera, J. Electroanal. Chem. 571 (2004) 15–26.
[29] A.S. Arico, G. Monforte, E. Modica, P.L. Antonucci, V. Antonucci, Electrochem. Commun. 2 (2000) 466–470.
[30] A.K. Shukla, A.S. Arico, K.M. El-Khatib, H. Kim, P.L. Antonucci, V. Antonucci, Appl. Surf. Sci. 137 (1999) 20–29.
[31] Y.M. Liang, H.M. Zhang, Z.Q. Tian, X.B. Zhu, X.L. Wang, B.L. Yi, J. Phys. Chem. B 110 (2006) 7828–7834.
[32] Z.B. Wang, G.P. Yin, Y.G. Lin, J. Power Sources 170 (2007) 242–250.
[33] H. Hoster, T. Iwasita, H. Baumgartner, W. Vielstich, J. Electrochem. Soc. 148 (2001) A496–A501.
[34] H. Hoster, T. Iwasita, H. Baumgartner, W. Vielstich, Phys. Chem. Chem. Phys. 3 (2001) 337–346.
[35] L.C. DeBolt, U.W. Suter, Macromolecules 20 (1987) 1425–1428.
[36] W.M. Chen, G.Q. Sun, Z.X. Liang, Q. Mao, H.Q. Li, G.X. Wang, Q. Xin, H. Chang, C. Pak, D. Seung, J. Power Sources 160 (2006) 933–939.
[37] A. Pozio, M. De Francesco, A. Cemmi, F. Cardellini, L. Giorgi, J. Power Sources 105 (2002) 13–19.
[38] C.L. Green, A. Kucernak, J. Phys. Chem. B 106 (2002) 1036–1047.
[39] J.H. Jiang, A. Kucernak, Chem. Mater. 16 (2004) 1362–1367.
[40] Z.B. Wang, H. Rivera, X.P. Wang, H.X. Zhang, X.P. Feng, E.A. Lewis, E.S. Smotkin, J. Power Sources 177 (2008) 386–392.
[41] A. Seo, J. Lee, K. Han, H. Kim, Electrochim. Acta 52 (2006) 1603–1611.
[42] D.R. Rolison, P.L. Hagans, K.E. Swider, J.W. Long, Langmuir 15 (1999) 774–779.